A NOVEL NONCONTACT ULTRASOUND INDENTATION SYSTEM FOR MEASUREMENT OF TISSUE MATERIAL PROPERTIES USING WATER JET COMPRESSION

M.H. Lu, Y.P. Zheng and Q.H. Huang

Jockey Club Rehabilitation Engineering Center, the Hong Kong Polytechnic University,

Kowloon, Hong Kong SAR, China.

Running Title: **Ultrasound Water Jet Indentation System**

Corresponding author:

Yongping Zheng

Jockey Club Rehabilitation Engineering Center,

The Hong Kong Polytechnic University,

Hung Hom, Kowloon, Hong Kong SAR, P. R. China.

Tel: 852-27667664

Fax: 852-23624365

Email: ypzheng@ieee.org

A NOVEL NONCONTACT ULTRASOUND INDENTATION SYSTEM FOR MEASUREMENT OF TISSUE MATERIAL PROPERTIES USING WATER JET COMPRESSION

M.H. Lu, Y.P. Zheng and Q.H. Huang

Jockey Club Rehabilitation Engineering Center, The Hong Kong Polytechnic University, Kowloon, Hong Kong SAR, China.

Abstract

This study is aimed to develop a novel noncontact ultrasonic indentation system for measuring quantitative mechanical properties of soft tissues, which are increasingly important for tissue assessment and characterization. The key idea of this method is to use a water jet as an indenter to compress the soft tissue while at the same time as a medium for an ultrasound beam to propagate through. The use of water jet indentation does not require a rigid compressor in front of the focused high frequency ultrasound transducer to compress the tissue, so that the additional attenuation caused by the rigid compressor and the strong echoes reflected from its surfaces can be avoided. The indentation deformation was estimated from the ultrasound echoes using a cross-correlation algorithm and the indentation force was calculated from the water pressure measured inside the water pipe. Experiments were performed on uniform tissue-mimicking phantoms with different stiffness. The Young's moduli and Poisson's ratios of these phantoms were measured using a uniaxial ultrasound compression system. The ratio of the indentation pressure to the tissue relative deformation was obtained from the water indentation. This ratio was well correlated with the Young's modulus (r=0.87). The results also demonstrated that the water indentation approach could differentiate materials with different stiffness in a combined phantom (288 kPa and 433 kPa). This novel noncontact water indentation approach could be potentially used for the measurement of

the elasticity of small samples and with a fast scanning speed. (E-mail: ypzheng@ieee.org)

Keywords: ultrasound, high-frequency ultrasound, indentation, ultrasound indentation, nanoindentation, noncontact, tissue, water jet.

INTRODUCTION

To measure or image the mechanical properties of tissues has been attracting increasing research efforts during the recent decades. The stiffness of soft tissues may change under different pathological situations, such as sclerous cancer, edema, degeneration, fibrosis and pressure sore (Mridha and Odman 1986, Garra et al. 1997). Normal tissues may also have different stiffness, which is important information for tissue characterization. The mechanical properties of tissues can have different values depending on whether they are measured *in vivo* or *in-vitro* and *in situ* or as an excised specimen (Fung 1981, Mow and Hayes 1997). For the lack of quantitative tools for *in vivo* assessment of living tissue, manual palpation has been the primary technique for tissue stiffness assessment for many years in clinic. However, it strongly relies on personal experiences and cannot provide a quantitative measurement of changes in tissue stiffness.

Many mechanical methods, such as indentation, compression, tension and torsion, are available quantitatively to measure the mechanical properties of soft tissues. Among them, indentation is one of the most frequently used approaches. It does not require special preparation for the specimens. Moreover, indentation can determine the material properties of soft tissues *in situ* or *in vivo*. Theoretical analysis of general indentation problems with various idealizations of the physical model has been conducted for about a century. Some mathematical solutions have also been reported for thin-layer soft tissues and materials using different mechanical model (Waters 1965; Hayes et al. 1972; Mak et al. 1987; Mow et al. 1989; Chicot et al. 1996; Yu and Blanchard 1996; Sakamoto et al. 1996; Haider and Holmes 1997). The indentation depth, the shape and size of the indenter, tissue thickness and the boundary conditions are critical factors in the calculation of tissue mechanical properties (Jurvelin et al. 1990; Suh and Spilker 1994; Zhang et al. 1997; Yang 2003).

Several generations of indentation instruments have been developed for the assessment of tissue mechanical properties, especially for articular cartilage (Kempson et al. 1971; Hori and Mockros 1976; Mow et al. 1989; Newton et al. 1997; Arokoski et al. 1994, 1999; Athanasiou et al. 1995, 1999; Shepherd and Seedhom 1997). These mechanical indentation apparatuses employ a load cell to measure the loading force and a displacement transducer (LVDT) to record the tissue deformation according to the displacement of the indenter. Cylindrical flat-ended and spherical indenters have been used to perform contact loading on soft tissues. The structures of these mechanical indentation instruments are complicated and not convenient for *in vivo* measurement. In addition, these instruments employ a needle probe to penetrate into the cartilage to measure the tissue thickness, which is important information for the estimation of stiffness. Destruction of the tissue structure at the site of measurement restricts the further use of the specimen. For clinical application, similar but portable indentation instruments have been developed for the quantification of cartilage stiffness under arthroscopic control (Lyyra et al. 1995), *in vivo* analysis of residual limb tissues (Pathak et al. 1998), plantar tissue stiffness measurement in patients with diabetes mellitus and peripheral neuropathy (Klaesner et al. 2002), stiffness estimation of spinal tissues (Kawchuk and Fauvel 2001) and heel pad stiffness assessment (Rome and Webb 2000). These indentation apparatuses use the obtained force/deformation (F/D) curves to indicate the tissue stiffness. However, the obtained stiffness may depend on the tissue thickness, which cannot be measured using these instruments.

During recent decades, ultrasound techniques together with compression or indentation have been successfully used for the measurement or imaging of the mechanical properties of soft tissues (Wilson and Robinson 1982; Ophir et al. 1991, Zheng and Mak 1996, Hsu et al. 1998, Adam et al. 1998, Suh et al. 2001, Kawchuk et al. 2000, Laasanen et al. 2002, Han et al. 2003). The ultrasound indentation apparatuses can simultaneously measure the tissue thickness and the tissue deformation *in vivo* noninvasively. A load cell or a strain gauge integrated with a flat-ended ultrasound transducer is used to collect the load applied on the tissue. In ultrasound indentation, the ultrasound transducer also serves as the indenter. The accuracy of ultrasonically-measured displacement during indentation has been earlier investigated (Zheng and Mak 1996, Kawchuk and Elliott 1998, Kawchuk et al. 2000). Compared with other methods, such as those using optical (Jurvelin et al. 1997) and needle probe (Mow et al. 1989) based methods, ultrasound-based techniques have proven to be most suitable for *in vivo* tissue thickness measurement, because of their noninvasiveness. Ultrasound indentation is easy to use for *in vivo* stiffness measurement and it has been widely used for assessment of normal limb tissues (Zheng and Mak 1999a, 1999b), residual limb tissues (Zheng et al. 1999), diabetic foot tissue (Zheng et al. 2000a, Hsu et al. 2000), fibrotic neck tissue induced by radiotherapy (Zheng et al. 2000b; Leung et al. 2002), spinal tissues (Kawchuk et al. 2001) and articular cartilage (Suh et al. 2001; Laasanen et al. 2002).

Present ultrasound indentation techniques utilize an unfocused transducer as the indenter to compress the soft tissue. Direct contact between the transducer and the specimen makes it difficult for them properly to compress small tissue specimens, due to the relatively large size of the transducer. Moreover, the reported ultrasound indentation device typically operated in the ultrasound frequency range of 2 MHz to 10 MHz. The resolution is not sufficient for the measurement and imaging of the mechanical properties of tissues with fine structures, such as articular cartilage (Zheng et al. 2002), corneal tissues (Hollman et al. 2002) or skin (Zheng et al. 2004). To achieve ultrasound indentation measurement at a microscopic level, ultrasound transducers with high frequency have to be used. An additional rigid compressor or indenter between the concave-faced focused transducer and the specimen is necessary for present techniques. The rigid indenter will attenuate the ultrasound signal significantly and generate multiple reflection signals which could overlap with signals from the specimen (Zheng et al. 2002, 2004). In addition, a contact compression or indentation could not allow for a fast scanning for a region of tissues. Accordingly, it is very necessary to develop a new method to achieve noncontact ultrasound indentation so that we can 1) perform proper loading on small specimen, 2) use high frequency ultrasound without the problem of high attenuation and 3) conduct a fast scanning to map tissue properties. Water jet acoustic coupling is well known in the nondestructive evaluation field for quality control (Birks and Green 1991; Zhao et al. 2003). Our approach is based on this technique. The key idea is to use a water jet simultaneously as the indenter and the medium for ultrasound to propagate through, so as to measure or map the mechanical properties of tissues. The potential of this noncontact ultrasound indentation system quantitatively to measure the phantoms with different stiffness is demonstrated in the following sections.

MATERIALS AND METHODS

Water indentation system

A noncontact ultrasound indentation system was constructed (Fig. 1), using a water jet as an indenter. As shown in Fig. 1, a bubbler (B120, GE Panametrics, Inc., West Chester, OH, USA) was used to eject a water jet by controlling the water flow. The diameter of the water-ejecting nozzle was 1.94 mm. A 20 MHz focused ultrasound transducer (model V316B, GE Panametrics, Inc., West Chester, OH, USA) was fixed with the bubbler, i.e., the water ejector and the focused ultrasound beam could propagate through the bubbler when it was full of water as coupling medium. The transducer and the bubbler were installed to a three-dimensional translating device (Parker Hannifin Corporation, Irvine, CA, USA) which was used to adjust the distance from the nozzle to the specimen surface and later was used to perform one-dimensional or two-dimensional scanning over the tissue. Specimens were placed on a rigid platform within a water container. An outlet on the side of the container was used to control the water level. A pressure sensor (EPB-C12, Entran Devices, Inc., Fairfield, NJ, USA) was used to measure the water pressure within the water pipe. A load cell (ELFS-T3M, Entran Devices, Inc., Fairfield, NJ, USA) located under the platform could sense the overall force applied on the specimen.

An ultrasound pulser/receiver (model 5052 UA, GE Panametrics, Inc. West Chester, OH, USA) was utilized to drive the ultrasound transducer and to amplify the received signal. The ultrasound echoes reflected from the specimen were digitized by a high speed A/D converter with a sampling rate of 2 GHz (Gage CS82G, Gage Applied Technologies, Inc**.,** QC, Canada). The pressure and the force were collected by a data acquisition card (DAQ 6024E, National Instruments Corp. Austin, TX, USA). Figure 2 shows the system diagram. A program has been developed in Microsoft VC++ to control the 3D translating device and collect, process and display the ultrasound signal, together with the force and the pressure, in real time during the indentation process. The user interface of the software is shown in Fig. 3. The acquisition of the A-mode ultrasound, force and pressure data was synchronized by the program. All the data could be recorded in a file for further off-line analysis. The deformation of the specimen under water jet indentation was estimated from the ultrasound echoes using a cross-correlation algorithm (Zheng et al. 2002). With the high-speed A/D converter, when the sampling frequency of 500 MHz was selected, the sensitivity of the time measurement was 2 ns. The theoretical sensitivity of the deformation determined by the water indentation system was better than 4 μm (Zheng et al. 2004). By using the 24-bit A/D converter to digitize the force and pressure signals, the accuracy of force was better than 1 μN within the 10 N range and the accuracy of pressure was better than 0.05 Pa within the 350 kPa range.

The pressure sensor was used to measure and monitor the water pressure within the water pipe. It was calibrated using a blood pressure meter with a range of 45 kPa and at a sensitivity of 0.13 kPa. The load cell could sense the overall force applied on the platform that was directly related to the force applied on the specimen by the water jet. It was calibrated by using an electronic balance with a range of 1 N and at a sensitivity of 0.1 mN. Both the pressure and the force were used to derive the pressure applied on the specimen by the water jet. The relationship between the overall force applied on the platform and the pressure within the water pipe was studied when the distance from the nozzle to the surface of the platform was fixed at approximately 5 mm, according to the focal length of the focused ultrasound transducer. A linear regression was used to study their relationship.

Phantom preparation

It has been reported that tissue-mimicking phantoms made from silicones or gels have similar mechanical properties with soft tissues and their shapes, sizes and compositions are easier to control (Hall et al. 1997). In our experiments, Rhodia RTV

573 (Rhodia Inc. CN7500, Cranbury, NJ, USA) and Wacker M4648 and M4640 silicones (Wacker Chemicals Hong Kong Ltd., HK, China) were used to make phantoms with different stiffness (Fig. 4). The uniform phantom was made from one kind of silicone and was supposed to be homogeneous. The combined phantom was made from two kinds of silicones, which had different stiffness at different areas. The sizes of the uniform phantoms were $1\times1\times0.5$ cm^3 (width×length×height), $1\times1\times1$ cm^3, $1\times1\times1.5$ cm^3. The combined phantoms had a height of 0.5 cm and a diameter of 2.2 cm.

Experiment design for the uniform phantom

To demonstrate the feasibility and the function of the noncontact ultrasound indentation system, experiments were performed on phantoms and the pressure/deformation curves were obtained. Galbraith and Bryant (1989) reported that the results of the indentation analysis were unaffected if the lateral dimension of the tissue was three or more times larger than the radius of the indenter. In this study, the lateral dimension of the phantom (1×1 cm^2) was more than five times the radius of the water indenter and the indentation was usually performed at the center of the phantom. During the test, the phantom was placed at the center of the platform and was gently fixed at edges by four screws. The position of the ultrasound transducer to the phantom surface was adjusted according to the height of the phantom, so as to keep a constant initial distance between the transducer and the phantom surface. The focal point of the transducer was placed approximately at the surface level of the phantom. The distance between the nozzle and the surface of the specimen was 5 mm. The container was full of water before loading and a constant water level was kept during the test. In each loading and unloading cycle, the water pressure within the water pipe was changed at a rate of approximately 45 kPa/s and from 0 to 180 kPa, which corresponds to the local deformation from 0 to approximately 0.4 mm for the softest phantom that we used. This process was repeated for three cycles in each test. Each phantom was indented three times. A total of 27 pieces of uniform phantoms were tested.

1-D scanning on the combined phantom

One-dimensional scanning experiment was conducted on the combined phantom, using the three-dimensional translating device. The phantom was first scanned by the ultrasound transducer at a moving rate of 1 mm/s when the pressure was kept as 0 kPa. Then it was scanned again along the same line after the pressure changed to 58 kPa. The deformation of the phantom at each site along the scanned line was obtained.

Measurement of mechanical properties of phantoms

As a reference of the experimental results of the water indentation, the compressive properties of the phantoms were measured using a mechanical testing device as shown in Fig. 5 (Zheng et al. 2002). The axial displacement was monitored by a displacement transducer-linearly variable differential transformer (LVDT) and the lateral deformation of the phantom was measured by an unfocused ultrasound transducer (5 MHz, model V316B, GE Panametrics, Inc. West Chester, OH, USA) during the axial compression. Similar technique for measuring the lateral displacement of articular cartilage has been reported by Fortin et al. (2003). Ultrasound coupling gel was used between the ultrasound transducer and the phantom for ultrasound beam propagation. It was also used in the interface between the phantom and the compressor and that between the phantom and the platform, serving as lubrication. The phantom was placed at the center of the platform and kept perpendicular to the ultrasound transducer by moving the phantom to obtain a maximal ultrasound echo reflected from the two opposite surfaces of the phantom. The ultrasound echoes were tracked using the cross-correlation algorithm to estimate the lateral deformation of the phantom during compression. The uniaxial force applied on the phantom was measured by a load cell (ELFS-T3M, Entran Devices, Inc., Fairfield, NJ, USA, calibrated for a range of 10 N). The axial displacement, force and ultrasound echoes were recorded synchronously by the program. The compressive Young's modulus and Poisson's ratio of the phantoms could be thus obtained.

The compressive Young's modulus of the phantom was calculated using eqn (1):

$$E = \frac{F/A}{\Delta L/L_0} \qquad (1)$$

where E is the compressive Young's modulus of the phantom, F is the axial force applied on the phantom, A is the surface area of the phantom, ΔL is the axial deformation and L_0 is the initial height of the phantom.

The Poisson's ratio calculation was based on the lateral deformation estimated from the ultrasound echoes and the axial deformation measured by LVDT (eqn (2)). A similar approach for the measurement of Poisson's ratio of articular cartilage using optical detection has been reported earlier (Jurvelin et al. 1997).

$$\upsilon = \frac{\Delta W/W_0}{\Delta L/L_0} = \frac{|W_1 - W_0|/W_0}{|L_1 - L_0|/L_0} \qquad (2)$$

where $W_0 = \frac{1}{2}t_1 \cdot c_{phantom}$, $W_1 = \frac{1}{2}t_2 \cdot c_{phantom}$, $\Delta W = W_1 - W_0 = \frac{1}{2}(t_2 - t_1) \cdot c_{phantom}$, where υ is the Poisson's ratio of the phantom, ΔW is the lateral deformation, ΔL is the axial deformation, W_0 and L_0 are the initial width and height of the phantom, t_1 and t_2 are the time of flight of ultrasound between the two lateral faces of the phantom before and after compression, respectively, and $c_{phantom}$ is the speed of sound in phantom. The meanings of these variables are shown in Fig. 6.

The test for each phantom included loading and unloading phases. The test was repeated three times on each phantom. The compression rate was kept at approximately 45 µm/s and the total deformation was up to 10%. Only the data with deformation less than 3% were used to calculate the Poisson's ratio and Young's modulus, corresponding to the 3% local strain of the phantoms under water indentation. According to the stress/strain curves of the phantoms obtained from compression, they were in the linear elastic region for the 3% deformation.

RESULTS

The mechanical properties of the phantoms were found to be dependent on the applied strain. Therefore, the Young's moduli and Poisson's ratios were measured at the strain according to the indentation depth on each phantom by using the noncontact water indentation system. The results showed a good repeatability with *ICC*=0.99 (intraclass correlation coefficient, SPSS Inc. Chicago, IL, USA) for the measurement of Young's moduli and *ICC*=0.98 for the measurement of Poisson's ratio, respectively. The Young's modulus of the phantoms ranged from 273 to 522 kPa and their Poisson's ratio ranged from 0.26 to 0.44. It was noted that the phantoms could have different moduli, even when they were made from the same silicone materials.

The calibration measurements indicated highly linear responses for both pressure and force transducers ($R^2 = 0.999$ for the pressure sensor; $R^2 = 0.998$ for the load cell). Moreover, it was found that there was a linear relationship ($R^2 = 0.99$) between the force applied on the platform collected by the load cell and the water pressure within water pipe measured by the pressure sensor (Fig. 7). Such a relationship will help us to investigate the pressure applied on the phantom surface. At present, the average pressure at the interface was calculated by the overall force divided by the initial contact area at the interface.

Figure 8a shows the pressure/deformation curves during the loading and unloading cycles applied on the phantom A and Fig. 8b shows the relationship between the pressure and the surface deformation of the phantom. The relationship between the deformation of the phantom and the applied water pressure loading was linear and the data were fitted using linear regression (average $R^2 = 0.99$). The obtained slope, i.e., the ratio of the applied pressure to the relative deformation, was defined as the stiffness ratio of the phantoms, with a unit of kPa. The measurements of the stiffness ratio of the phantoms showed a good repeatability (*ICC*>0.99) for the three tests. The stiffness ratio of the phantoms ranged from 1582 to 4269 kPa.

A good linear relationship between the compressive Young's moduli and the stiffness ratios was found with the correlation coefficient $r = 0.87$ ($n = 27$) (Fig. 9). This result demonstrated that the ultrasound water indentation system had the ability quantitatively to measure the phantoms with different stiffness. We estimated the Young's modulus, E_w, from the obtained relationship between the stiffness ratio and the compressive Young's modulus, E, of the phantoms. A Bland-Altman plot (Fig. 10) was added to give indication of the size of errors between E_w and E. The mean difference $\bar{d}$ was 0.02 kPa and the standard deviation s was 35.43 kPa. From the Bland-Altman plot, most of the differences lay between $\bar{d} - 2s$ and $\bar{d} + 2s$. The result was acceptable for clinical applications (Bland and Altman, 1986). The thickness of the phantom was also significantly ($P < 0.001$, linear regression by SPSS) correlated with the Young's modulus.

Moreover, significant correlation between the stiffness ratios and the square of Poisson's ratios was found (P = 0.04). However, the extraction of the intrinsic mechanical properties of the test materials from the water indentation needs further investigations.

Figure 11a shows the comparison of the M-mode ultrasound images obtained under two different pressures (0 and 58 kPa). It could be observed that the surface of the combined phantom was not flat. Figure 11b is the deformation distribution along the scanned line derived from Fig. 11a. The result showed that, under a certain pressure, the deformation of the region made from material A was larger than that made from material B, i.e., the region made from material A was softer than that made from material B. The Young's modului of these two regions were 288±2 and 433±5 kPa, respectively. The measured deformation distribution under a certain pressure well demonstrated the stiffness distribution of the combined phantom. We used this preliminary result to demonstrate the feasibility of using the water indentation to map the distribution of the stiffness ratio of soft tissues.

DISCUSSION AND CONCLUSION

A noncontact ultrasound indentation system using water jet has been developed for the assessment of tissue mechanical properties. Preliminary results have demonstrated that this novel system was feasible quantitatively to measure silicone phantoms with different stiffness. As a water jet was used simultaneously as the indenter and the medium for coupling the ultrasound beam, the system could obtain better ultrasound echoes using focused high frequency ultrasound in comparison with the contact methods, where rigid indenters or compressors were used to compress the tissue. It could also conduct proper loading on small specimen, because of the small dimension of the water indenter. Moreover, this water jet indentation system demonstrated its potential to conduct fast scanning on specimens to map the deformation distribution.

In our experiments, a 20 MHz focused ultrasound transducer was used and the system could achieve high axial resolution of the measurement because the deformation of phantom under water indentation was determined from ultrasound echoes. For 20 MHz ultrasound using in this study, two cycles of damping period and an ultrasound speed of 1480 m/s (Krautkramer and Krautkramer 1969), the theoretical axial resolution was approximately 58 μm (Bushong and Archer 1991, Foster et al. 2000). The focal length of the transducer was 19.05 mm, and the diameter of the active element of this transducer was 3.175 mm. Therefore, the f-number (focal length/crystal diameter) was 6. The theoretical lateral resolution was 0.44 mm (Foster et al. 2000). The resolutions could be further improved by using higher frequency ultrasound. According to the numerical simulation results, Righetti et al. (2002, 2003) and Srinivasan et al. (2003) reported that the lateral and axial resolution limits of the strain images obtained using ultrasound were on the order of the sonographic lateral resolution and the ultrasonic wavelength, respectively. In the future study on the small specimen of soft tissues, a focused 50 MHz ultrasound transducer will be used and it can achieve a theoretical axial resolution of 35 μm, and lateral resolution of 90 μm (Zheng et al. 2004). With further improvement of the system, it is feasible to perform nanoindentation (Pethica et al. 1983) using the water indentation. In the present study, we have only focused on the ultrasound echoes reflected from the phantom surface, from which the overall deformation was derived. For the tissues with multilayer or inhomogeneous structures, echoes from different depths can be tracked during water indentation so as potentially to map the tissue stiffness in the depth direction. Further experiments are required to validate the stiffness distribution using proper techniques such as the optical elastomicroscopy system (Huang et al. 2004).

In our experimental set-up, daily tap water (24.2±0.2ºC) was used for the water indentation system. We are planning to use a water pump, so that the water flow can be better controlled. As the medium for ultrasound propagation was flowing during the water indentation, the effect of the flow rate on the ultrasound speed had to be investigated. Our result showed that the maximal change of the speed of sound through water jet was less than 0.04% (0.6 m/s change for a speed of 1480 m/s) when the pressure was changed from 0 to 180 kPa. The result suggested that the effect of water flow for ultrasound speed could be neglected during the water indentation with the pressure up to 180 kPa. The water jet formed from the tap water might contain some amount of air bubbles. The backscatter induced by these bubbles may attenuate the ultrasonic beam that propagates through the water jet. It has been reported that the attenuation caused by the air bubbles increases rapidly as the frequency is increased (Ophir and Parker 1989, Naito et al. 1998, Phillips et al. 1998). However, the effects of the bubbles to the test proposed in this study could be negligible according to our measurement. No dramatic attenuation and scattering was caused by the air bubbles in the set-up used in this study. For the 20 MHz ultrasonic beam, we noted that the ultrasound echo from a steel plate located at the focal zone was attenuated by less than -0.6 dB when the water flow was adjusted from 0 to the maximum value that used in this study. Such a small attenuation to the echo was negligible in this study, as the main information involved in the calculation of the deformation was the flight-time of the echo reflected from the surfaces of the phantom.

During our experiments, the ratio between the pressure and the relative deformation curves was used as the index of the material stiffness. The stiffness ratio had a good linear relationship (with correlation coefficients larger than 0.8) with the measured compressive Young’s modulus. This correlation may not be good enough for a very precise measurement. However, the result demonstrated the feasibility of the new ultrasound water jet system to measure the stiffness of the phantoms quantitatively. The result of Bland-Altman plot (Fig. 10) demonstrated that the results were acceptable for clinical applications (Bland and Altman, 1986).

However, the extraction of the intrinsic mechanical properties from the noncontact water indentation needs further investigation. As previous investigations have suggested (Waters, 1965; Hayes et al. 1972; Mak et al. 1987; Mow et al. 1989; Chicot et al. 1996; Yu and Blanchard, 1996; Sakamoto et al. 1996; Haider and Holmes, 1997), the Young's modulus derived from indentation test using a cylindrical indenter is related to the Poisson's ratio of the material, stress distribution, indentation depth and tissue thickness. Moreover, when soft tissues are tested for the measurements of mechanical properties, the nonlinearity, viscoelasticity, nonhomogenuity and anisotropy should be carefully considered for the mechanical properties' extraction. In this study, as the first step, we tested silicone phantoms with uniform structures. The applied deformation was within 3% and the loading cycle was completed within 4 s, so as to reduce the effects of nonlinearity and viscoelasticity. We used the slope of the pressure/ relative deformation curve instead of the pressure/ deformation curve to correlate with the Young's modulus, since we found that the thickness of the phantoms was also well correlated with their stiffness. Moreover, significant correlation between the stiffness ratio and square of Poisson's ratio was also found. These observations will benefit us further to investigate the extraction of intrinsic material parameters from the water indentation results. However, we were not able yet to obtain a suitable equation precisely to describe the relationship between the Young's modulus and the Poisson's ratio, tissue thickness, as well as the applied pressure and the indentation depth using our experimental data.

The major cause of the discrepancy between the stiffness ratios measured using the water jet indentation method and the Young's moduli measured using the compression method may be the simplification in modeling the interaction between the water jet and the phantom surface. It is expected that the deformation profile as well as the pressure distribution along the interacting interface keeps changing as the increase of the water jet pressure. We have tried different methods to measure the deformation profile and the pressure distribution. However, no satisfactory results have been obtained yet. In addition to improving our experimental approaches, we are also planning for the numerical analysis of the interaction between the water jet and the tissue. Finite element analysis is an effective tool and it has been employed to study the indentation problem (Galbraith and Bryant 1989; Jurvelin et al. 1990; Zhang et al. 1997; Lu and Zheng 2004). Using finite element analysis, we expect that the effects of the variations of the water jet radius, the distance from the nozzle to the phantom surface, the phantom thickness and the Poisson's ratio and the fluid-solid coupling motion can be studied. The interaction between the water jet and the tissue can be better investigated.

This noncontact ultrasound water indentation system has many potential applications. With further improvement of the system and better understanding about the water jet-tissue interaction, we expect that the water indentation approach could be potentially used quantitatively to assess the stiffness of body tissues for clinical diagnosis, such as skin cancer, burn status, cornea condition, blood vessel stiffening, articular cartilage degeneration etc. It could also be employed to perform indentation on small specimens in microscopic levels for tissue and material characterization for small animal tissues, bioengineered tissues, semiconductor materials, thin films and so on, where nanoindentation is widely used. Moreover, the potential fast scanning feature of the water indentation makes it easy to conduct scanning on tissues with large area.

Acknowledgements

This work was partially supported by the Research Grants Council of Hong Kong (PolyU 5245/03E) and The Hong Kong Polytechnic University.

REFERENCES

Adam C, Eckstein F, Milz S, Schulte E, Becker C and Putz R. The distribution of cartilage thickness in the knee-joints of old-aged individuals - measurement by A-mode ultrasound. Clin Biomech 1998; 13: 1-10.

Arokoski JPA, Hyttinen MM, Helminen HJ and Jurvelin JS. Biomechanical and structural characteristics of canine femoral and tibial cartilage. J Biomed Mater Res 1999; 48: 99-107.

Arokoski J, Jurvelin J, Kiviranta I, Tammi M and Helminen HJ. Softening of the lateral condyle aricular-cartilage in the canine knee-joint after long-distance (up to 40 km/day) running training lasting one-year. Int J Sports Med 1994; 15: 254-260.

Athanasiou KA, Agarwal A, Muffoletto A, Dzida FJ, Constantinides G and Clem M. Biomechanical properties of hip cartilage in experimental animal-models. Clin Orthop Relat R 1995; 316: 254-266.

Athanasiou KA, Fleischli JG, Bosma J, et al. Effects of diabetes mellitus on the biomechanical properties of human ankle cartilage. Clin Orthop Relat R 1999; 368: 182-189.

Birks AS and Green RE. Ultrasonic testing: nondestructive testing handbook. 1991; Columbus, OH: American Society for Nondestructive Testing, Inc.

Bland JM and Altman DG. Statistical methods for assessing agreement between two methods of clinical measurement. Lancet 1986; i: 307-310.

Bushong SC and Archer BR. Diagnostic ultrasound: physics, biology, and instrumentation, 1991; New York: Mosby..

Chicot D, Hage I, Demarecaux P and Lesage J. Elastic properties determination from indentation tests. Surf Coat Tech 1996; 81: 269-274.

Galbraith PC and Bryant JT. Effect of grid dimensions on finite element models of an articular surface. J Biomech 1989; 22: 385-393.

Garra BS, Cespedea EI, Ophir J, Spratt RS, Zuurbier RA, Magnant CM, and Pennanen MF. Elastography of breast lesions: initial clinic results. Radiology 1997; 202: 79-86.

Fung YC. Biomechanical properties of living tissues. 1981; Springer-Verlag, New York.

Foster FS, Pavlin CJ, Harasiewicz KA, Christopher DA, and Turnbull DH. Advances in ultrasound biomicroscopy. Ultrasound Med Biol 2000; 26: 1-27.

Fortin M, Buschmann MD, Bertrand MJ, Foster FS, and Ophir J. Dynamic measurement of internal solid displacement in articular cartilage using ultrasound backscatter. J Biomech 2003; 36: 443-447.

Haider MA and Holmes MH. A mathematical approximation for the solution of a static indentation test. J Biomech 1997; 30: 747-751.

Hall TJ, Bilgen M, Insana MF and Krouskop TA. Phantom materials for elastography. IEEE T Ultrason Ferr 1997; 44: 1355-1365.

Han LH, Noble JA and Burcher M. A novel ultrasound indentation system for measuring biomechanical properties of in vivo soft tissue. Ultrasound Med Biol 2003; 29: 813-823.

Hayes WC, Herrmann G, Mockros LF and Keer LM. A mathematical analysis for indentation tests of articular cartilage, J Biomech 1972; 5: 541-551.

Hollman KW, Emelianov SY, Neiss JH, et al. Strain imaging of corneal tissue with an ultrasound elasticity microscope. Cornea 2002; 21: 68-73.

Hori RY and Mockros LF. Indentation tests of human articular-cartilage. J Biomech 1976; 9: 259-268.

Huang QH, Lu MH and Zheng YP. Optical and ultrasound elastomicroscopy for imaging tissue elasticity in high resolution. Conference on Biomedical Engineering, BME 2004, 23 -25 September 2004, Hong Kong: 130-134

Hsu TC, Wang CL, Shau YW, Tang FT, Li KL, Chen CY. Altered heel-pad mechanical properties in patients with Type 2 diabetes mellitus. Diabet Med 2000; 17: 854-859.

Hsu TC, Wang CL, Tsai WC, Kuo JK, and Tang FT. Comparison of the mechanical properties of the heel pad between young and elderly adults. Arch Phys Med Rehabil 1998; 79: 1101-1104.

Jurvelin J, Kiviranta I, Saamanen AM, Tammi M and Helminen HJ. Indentation stiffness of young canine knee articular-cartilage – influence of strenuous joint loading. J Biomech 1990; 23: 1239-1246.

Jurvelin JS, Buschmann MD and Hunziker EB. Optical and mechanical determination of Poisson's ratio of adult bovine humeral articular cartilage. J Biomech 1997; 30: 235-241.

Kawchuk GN and Elliott PD. Validation of displacement measurements obtained from ultrasonic images during indentation testing. Ultrasound Med Biol 1998; 24: 105-111.

Kawchuk GN and Fauvel OR. Sources of variation in spinal indentation testing: indentation site relocation, intraabdominal pressure, subject movement, muscular response, and stiffness estimation. J Manip physiol ther 2001a; 24: 84-91.

Kawchuk GN, Fauvel OR and Dmowski J. Ultrasonic quantification of osseous displacements resulting from skin surface indentation loading of bovine para-spinal tissue. Clin Biomech 2000; 15: 228-233.

Kawchuk GN, Fauvel OR and Dmowski J. Ultrasound indentation: a procedure for the noninvasive quantification of force-displacement properties of the lumber spine. J Manip physiol ther 2001b; 24: 149-156.

Kempson GE, Freeman MAR and Swanson SAV. The determination of a creep modulus for articular cartilage from indentation tests on human femoral head. J Biomech 1971; 4: 239-250.

Klaesner JW, Hastings MK, Zou DQ, Lewis C and Mueller MJ. Plantar tissue stiffness in patients with diabetes mellitus and peripheral neuropathy. Arch Phys Med Rehabil 2002; 83: 1796-1801.

Krautkramer J and Krautkramer H. Ultrasonic testing of materials. 1969; New York: Springer-Verlag.

Laasanen MS, Toyras J, Hirvonen J, et al. Novel mechano-acoustic technique and instrument for diagnosis of cartilage degeneration. Physiol Meas 2002; 23: 491-503.

Leung SF, Zheng YP, Choi CYK, et al. Quantitative measurement of post-irradiation neck fibrosis based on the Young modulus: description of a new method and clinical results. Cancer 2002; 95: 656-662.

Lu MH and Zheng YP. Indentation test of soft tissues with curved cubstrates: a finite element study. Med Biol Eng Comput 2004; 42: 535-540.

Lyyra T, Jurvelin J, Pitkanen P, Vaatainen U and Kiviranta I. Indentation instrument for the measurement of cartilage stiffness under arthroscopic control. Med Eng Phys 1995; 17: 395-399.

Mak AF, Lai WM and Mow VC. Biphasic indentation of articular-cartilage .1. theoretical -analysis. J Biomech 1987; 20: 703-714.

Mow VC, Gibbs MC, Lai WM, Zhu WB and Athanasiou KA. Biphasic indentation of articular-cartilage .2. a numerical algorithm and an experimental-study. J Biomech 1989; 22: 853-861.

Mow VC and Hayes WC. Basic Orthopaedic Biomechanics. 2nd edition. 1997; Lippincott-Raven.

Mridha M and Odman S. Noninvasive method for assessment of subcutaneous edema. Med Biol Eng Comput 1986; 24: 393-398.

Newton PM, Mow VC, Gardner TR, Buckwalter JA and Albright JP. The effect of lifelong exercise on canine articular cartilage. AM J Sport Med 1997; 25: 282-287.

Naito T, Ohdaira E, Masuzawa N, and Ide M. Relationship between cavitation threshold and dissolved air in ultrasound in the MHz range. Jpn J Appl Phys 1998; 37: 2990-2991.

Ophir J, Ce´spedes I, Ponnekanti H, Yazdi Y and Li X. Elastography: a quantitative method for imaging the elasticity of biological tissues. Ultrasonic Imaging 1991; 13: 111–134.

Ophir J and Parker KJ. Contrast agents in diagnostic ultrasound. Ultrasound Med Biol 1989; 15: 319-333.

Pathak AP, Silver-Thorn MB, Thierfelder CA and Prieto TE. A rate-controlled indentor for in vivo analysis of residual limb tissues. IEEE T Rehabil Eng 1998; 6: 12-20.

Pethica JB, Hutchings R, and Oliver WC. Hardness measurement at penetration depths as small as 20-nm. Philos Mag A 1983; 48: 593-606.

Phillips D, Chen XC, Baggs R, Rubens D, Violante M, and Parker KJ. Acoustic backscatter properties of the particle/bubble ultrasound contrast agent. Ultrasonics 1998; 36: 883-892.

Righetti R, Ophir J, and Ktonas P. Axial resolution in elastography. Ultrasound Med Biol 2002; 28: 101-113.

Righetti R, Srinivasan S, and Ophir J. Lateral resolution in elastography. Ultrasound Med Biol 2003; 29: 695-704.

Srinivasan S, Righetti R, and Ophir J. Trade-offs between the axial resolution and the signal-to-noise ratio in elastography. Ultrasound Med Biol 2003; 29: 847-866.

Rome K and Webb P. Development of a clinical instrument to measure heel pad indentation. Clin Biomech 2000; 15: 298-300.

Sakamoto M, Li GA, Hara T and Chao EYS. A new method for theoretical analysis of static indentation test. J Biomech 1996; 29: 679-685.

Shepherd DET and Seedhom BB. Technique for measuring the compressive modulus of articular cartilage under physiological loading rates with preliminary results. P I Mech Eng H 1997; 211: 155-165.

Suh JK and Spilker RL. Indentation analysis of biphasic articular-cartilage – nonlinear phenomena under finite deformation. J Biomech Eng- T ASME 1994; 116: 1-9.

Suh JKF, Youn I and Fu FH. An in situ calibration of an ultrasound transducer: a potential application for an ultrasonic indentation test of articular cartilage. J Biomech 2001; 34: 1347-1353.

Waters NE. The indentation of thin rubber sheets by spherical indentors. Brit J Appl Phys 1965; 16: 557-563.

Wilson LS and Robinson DE. Ultrasonic measurement of small displacements and deformations of tissue. Ultrasonic Imaging 1982; 4: 71–82.

Yang F. Thickness effect on the indentation of an elastic layer. Mat Sci Eng A 2003; 358: 226-232.

Yu WP and Blanchard JP. An elastic-plastic indentation model and its solutions. J Mater Res 1996; 11: 2358-2367.

Zhang M, Zheng YP and Mak AFT. Estimating the effective Young's modulus of soft tissues from indentation tests - nonlinear finite element analysis of effects of friction and large deformation. Med Eng Phys 1997; 19: 512-517.

Zhao B, Basir OA, and Mittal GS. A self-aligning ultrasound sensor for detecting foreign bodies in glass containers. Ultrasonics 2003; 41: 217-222.

Zheng YP, Bridal SL, Shi J, et al. High resolution ultrasound elastomicroscopy imaging of soft tissues: system development and feasibility. Phys Med Biol 2004; 49: 3925-3938.

Zheng YP, Choi YKC, Wong K, Chan S and Mak AFT. Biomechanical assessment of plantar foot tissue in diabetic patients using an ultrasound indentation system. Ultrasound Med Biol 2000a; 26: 451-456.

Zheng YP, Leung SF and Mak AFT. Assessment of neck tissue fibrosis using an ultrasound palpation system: A feasibility study. Med Biol Eng Comput 2000b; 38: 497-502.

Zheng YP and Mak AFT. An ultrasound indentation system for biomechanical properties assessment of soft tissues in-vivo. IEEE T Bio-Med Eng 1996; 43: 912-918.

Zheng YP and Mak AFT. Extraction of quasilinear viscoelastic parameters for lower limb soft tissues from manual indentation experiment. J Biomech Eng- T ASME 1999a; 121: 330-339.

Zheng YP and Mak AFT. Effective elastic properties for lower limb soft tissues from manual indentation experiment. IEEE T Rehabil Eng 1999b; 7: 257-267.

Zheng YP, Mak AFT, Lau KP and Qin L. An ultrasonic measurement for in vitro depth-dependent equilibrium strains of articular cartilage in compression. Phys Med Biol 2002; 47: 3165-3180.

Zheng YP, Mak AFT and Lue B. Objective assessment of limb tissue elasticity: development of a manual indentation procedure. J Rehabil Res Dev 1999; 36: 71-85.

Figure Captions

Fig. 1. Diagram of the noncontact ultrasound indentation system using water jet compression. The water jet is used as an indenter and focused high-frequency ultrasound is employed to monitor the deformation of the soft tissue. The dimensions of the important components are: nozzle diameter 1.94 mm, water supply pipe diameter 3 mm, platform diameter 24 mm, load cell diameter 12.7 mm, ultrasound transducer active

element diameter 3.175 mm and the distance from the nozzle to tissue approximately 5 mm.

Fig. 2. The water indentation and data collection diagram of the noncontact ultrasound water indentation system.

Fig. 3. The user interface of the signal processing software. The left column is the control panel, showing various parameters. In the main window, the lower right window displays the real-time ultrasound signal reflected from the sample surface, the lower left windows shows the force sensed by the load cell or pressure measured by the pressure sensor, the upper left window shows the M-mode ultrasound signals and the upper right window is the deformation extracted from the ultrasound signal using the cross-correlation tracking algorithm.

Fig. 4. Phantoms made from three kinds of silicones were prepared for the experiments. (a) The uniform phantoms with dimensions $1\times1\times0.5\ \text{cm}^3$ (width×length×height), (b) $1\times1\times1\ \text{cm}^3$ and (c) $1\times1\times1.5\ \text{cm}^3$. (d) The combined phantom with a height of 0.5 cm and a diameter of 2.2 cm.

Fig. 5. Diagram of the system which was used to measure the compressive Young's modulus and Poisson's ratio of the phantoms. A load cell was used to measure the uniaxial force applied on the phantom. An ultrasound transducer was used to estimate the lateral deformation of the phantom, while the LVDT was used to measure the axial deformation.

Fig. 6. Schematic diagram for the estimation of the Poisson's ratio of the uniform phantom. t_1 and t_2 are the times-of-flight of ultrasound from the two parallel surfaces of the phantom before and after compression, respectively.

Fig. 7. The relationship between the force applied on the platform and the pressure measured within the water pipe. The equation shows the result of a linear regression.

Fig. 8 (a). Pressure-deformation curves obtained during the loading and unloading cycles applied on one uniform phantom. (b) The relationship between the pressure measured within the water pipe and the relative deformation of the phantom.

Fig. 9. The correlation between the compressive Young's modulus and the stiffness ratio obtained using the ultrasound water indentation (r=0.87, n=27).

Fig. 10. Bland-Altman plot to test the agreement between the estimated Young's modulus by water indentation and the measured modulus by compression.

Fig. 11. A typical result of one-dimensional scanning on the combined phantom. (a) Comparison of the M-mode ultrasound images obtained under two different pressures. (b) The deformation distribution along the scanned line as derived from (a).

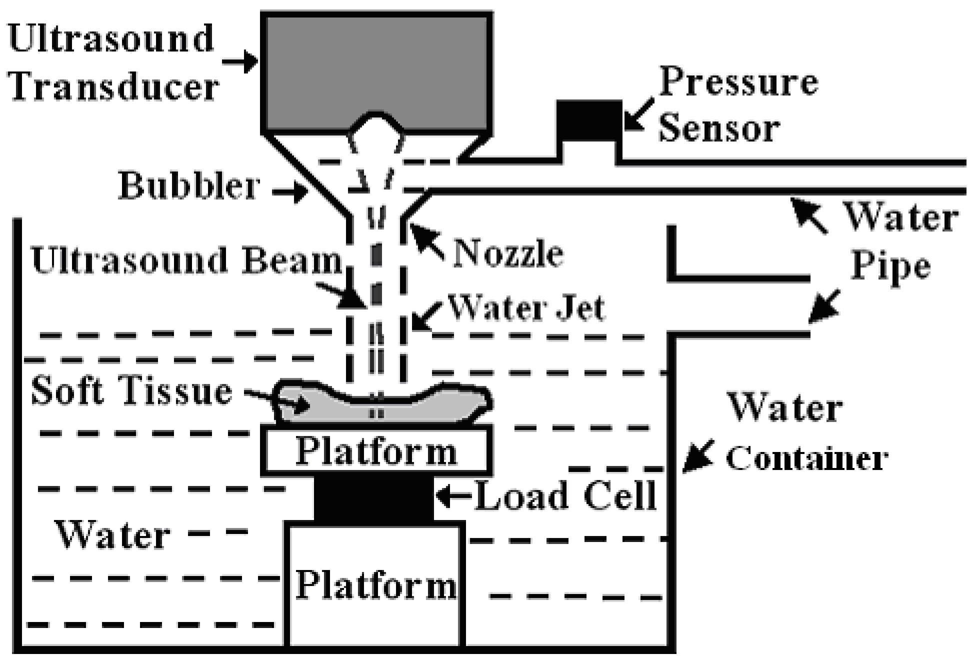
Ultrasound Transducer
Pressure Sensor
Bubbler
Water Pipe
Nozzle
Ultrasound Beam
Water Jet
Soft Tissue
Water Container
Platform
Load Cell
Water
Platform

Figure 1.

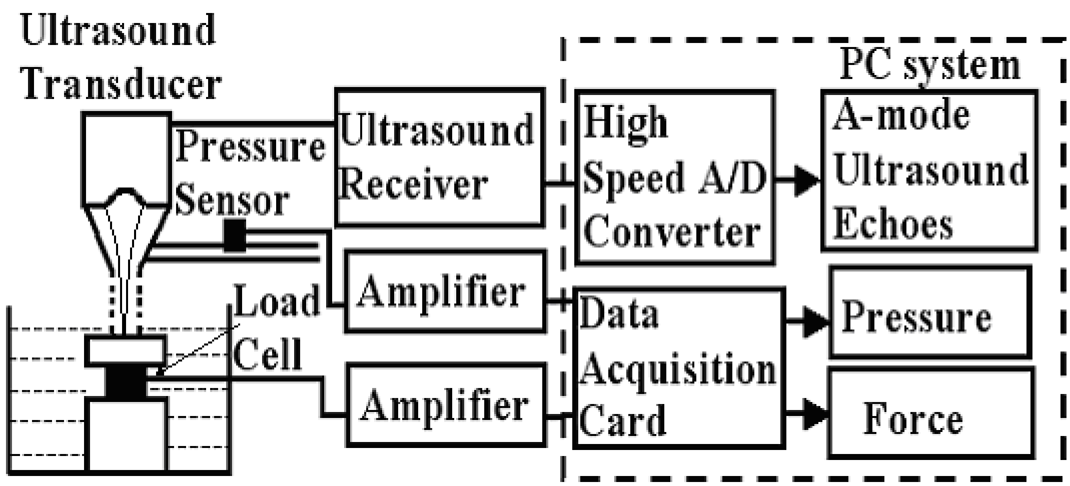
Ultrasound
Transducer
Pressure
Sensor
Ultrasound
Receiver
Amplifier
Load
Cell
Amplifier
PC system
High
Speed A/D
Converter
A-mode
Ultrasound
Echoes
Data
Acquisition
Card
Pressure
Force

Figure 2.

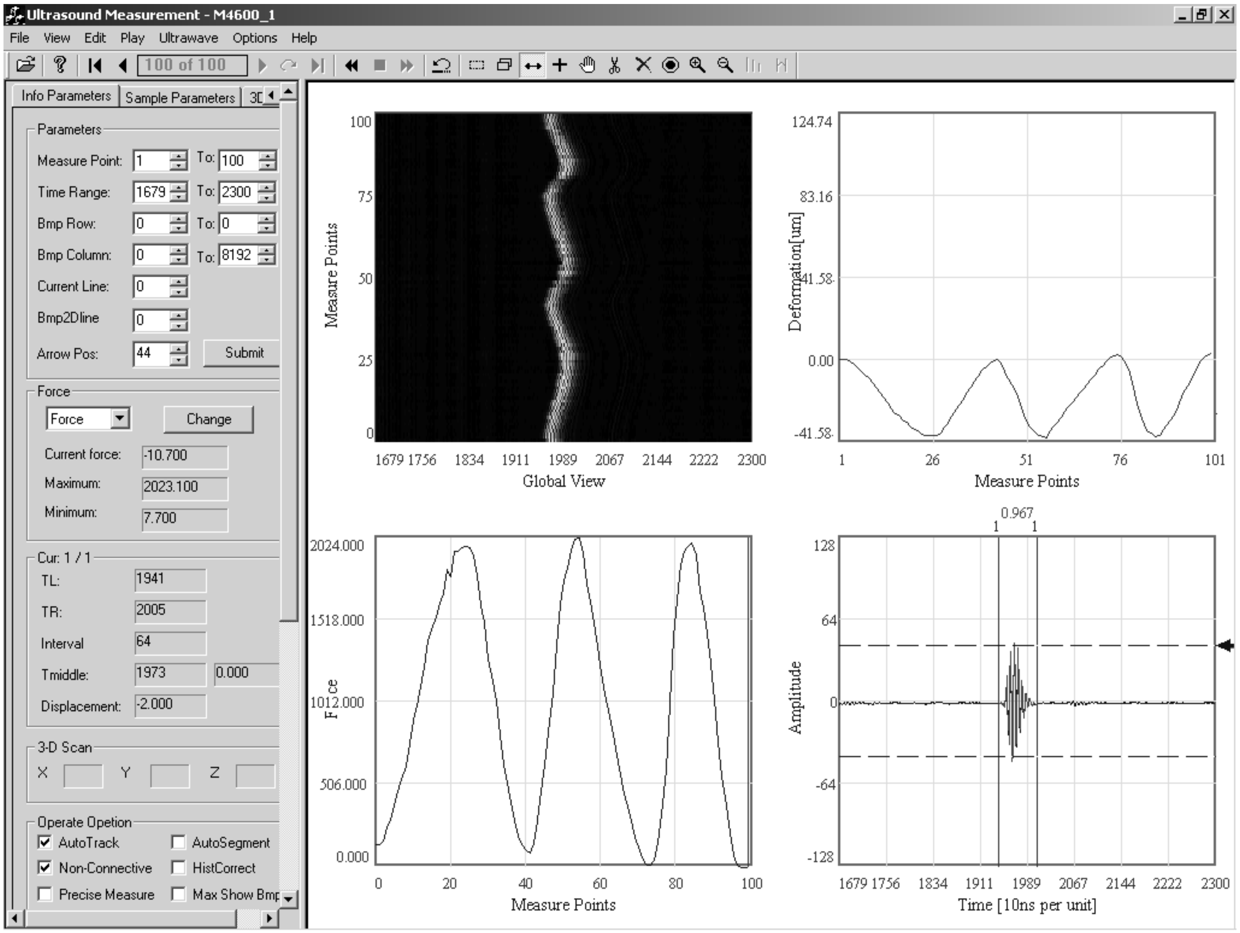
Ultrasound Measurement - M4600_1
File View Edit Play Ultrawave Options Help
100 of 100
Info Parameters
Sample Parameters
Parameters
Measure Point: 1 To: 100
Time Range: 1679 To: 2300
Bmp Row: 0 To: 0
Bmp Column: 0 To: 8192
Current Line: 0
Bmp2Dline 0
Arrow Pos: 44
Submit
Force
Force
Change
Current force: -10.700
Maximum: 2023.100
Minimum: 7.700
Cur: 1 / 1
TL: 1941
TR: 2005
Interval 64
Tmiddle: 1973 0.000
Displacement: -2.000
3-D Scan
X Y Z
Operate Opetion
AutoTrack
AutoSegment
Non-Connective
HistCorrect
Precise Measure
Max Show Bmp
Measure Points
Global View
Deformation[um]
Measure Points
Force
Measure Points
Amplitude
Time [10ns per unit]
0.967

Figure 3.

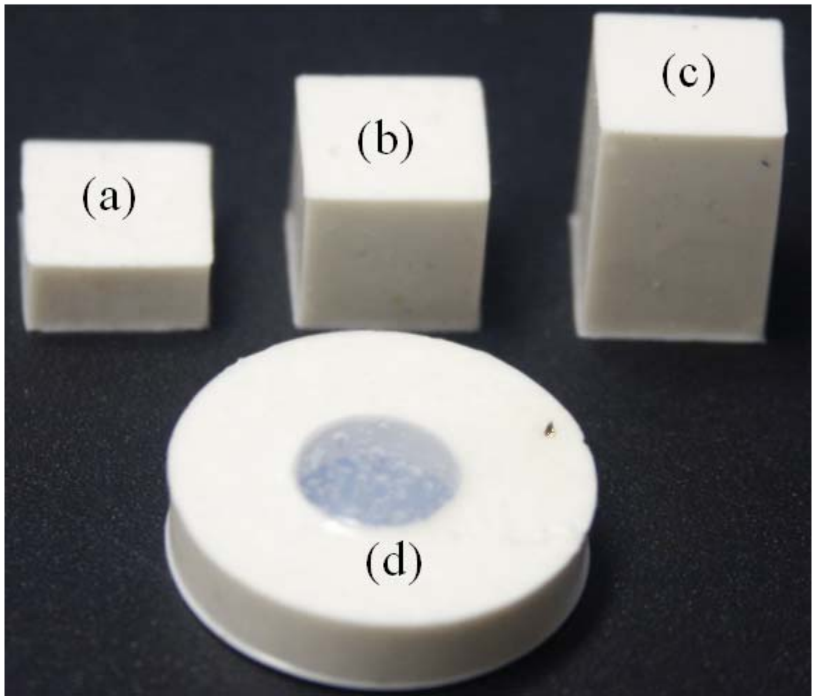

Figure 4.

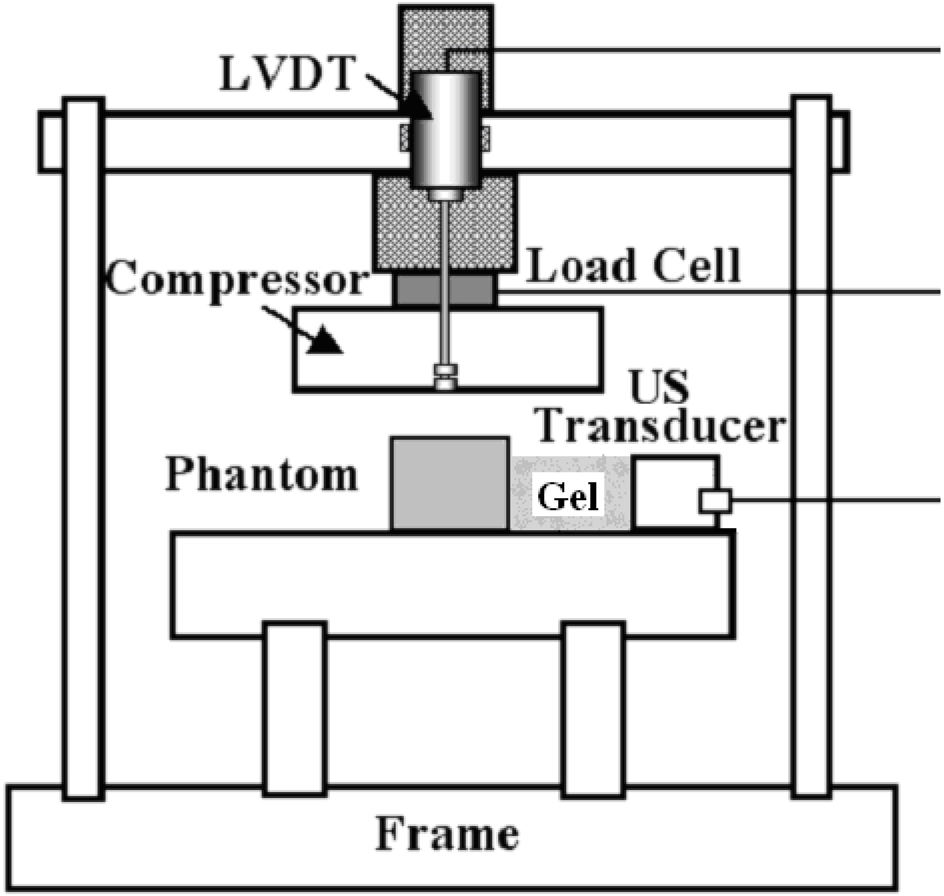

Figure 5.

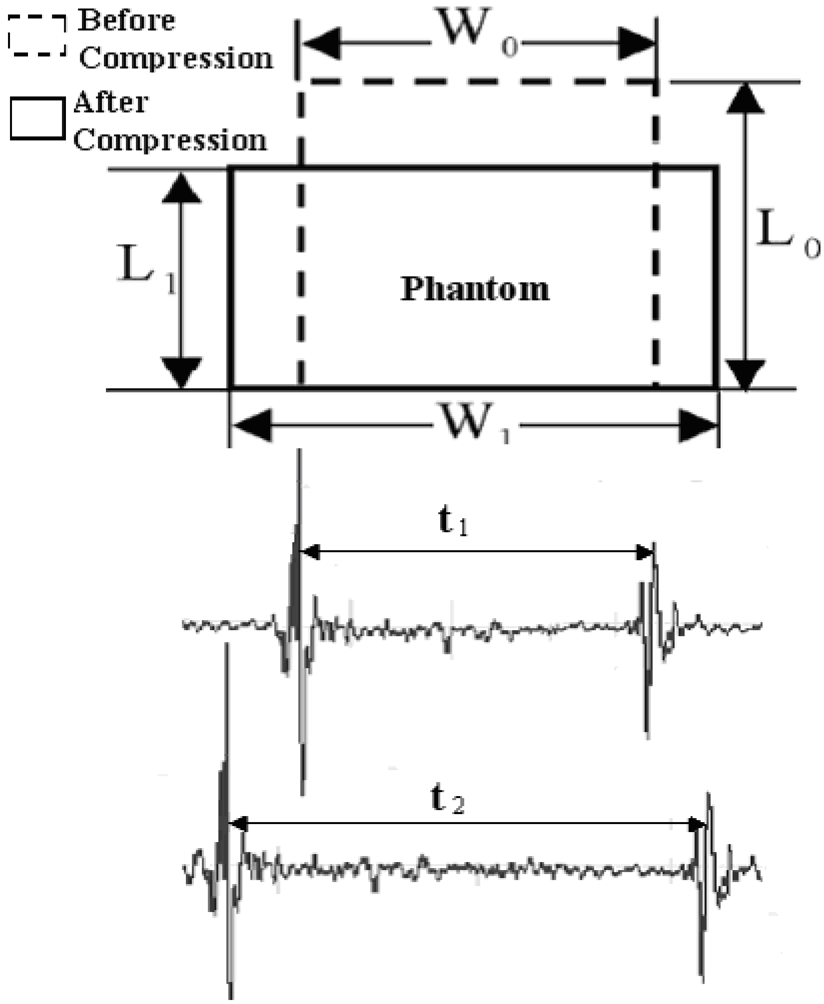
Before Compression
After Compression
W_0
L_0
L_1
Phantom
W_1
t_1
t_2

Figure 6.

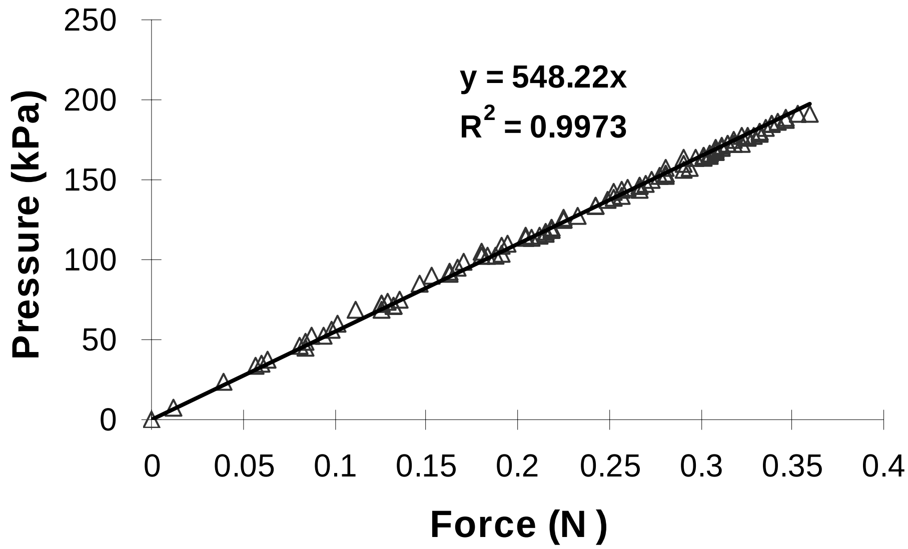
y = 548.22x
R2 = 0.9973
250
200
150
100
50
0
Pressure (kPa)
0
0.05
0.1
0.15
0.2
0.25
0.3
0.35
0.4
Force (N)

Figure 7.

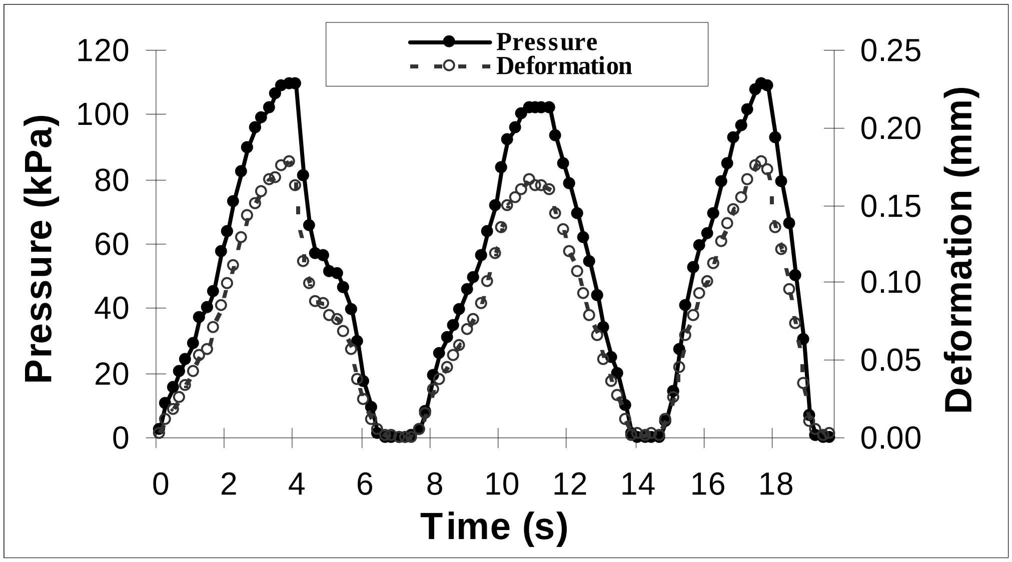

Figure 8 (a).

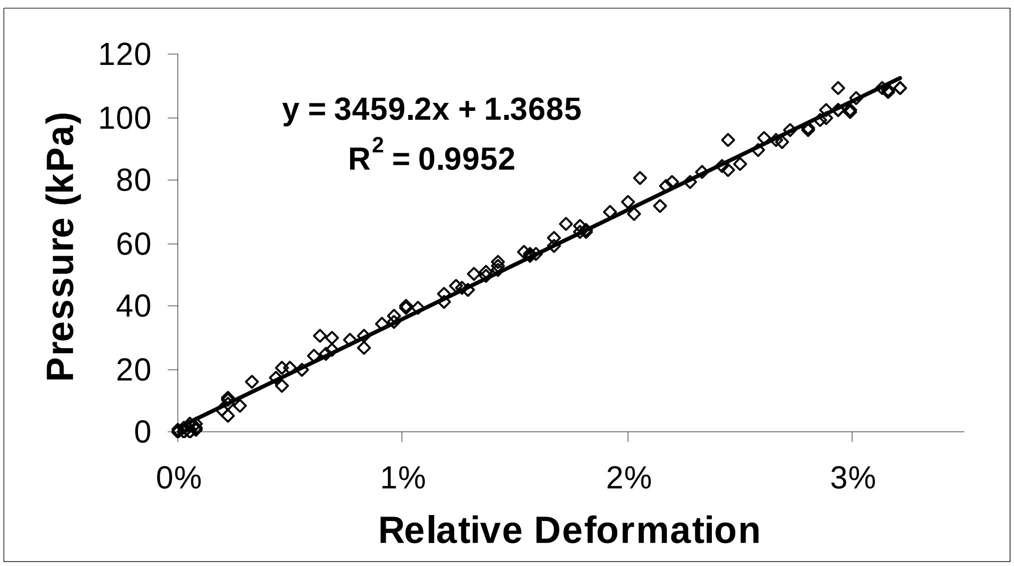

Figure 8 (b).

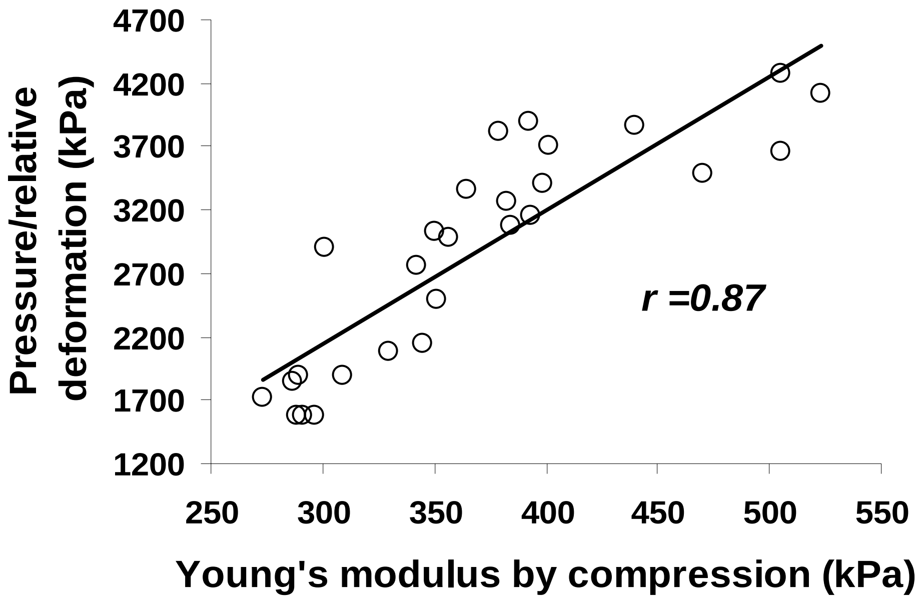
Pressure/relative deformation (kPa)
4700
4200
3700
3200
2700
2200
1700
1200
250
300
350
400
450
500
550
Young's modulus by compression (kPa)
r =0.87

Figure 9.

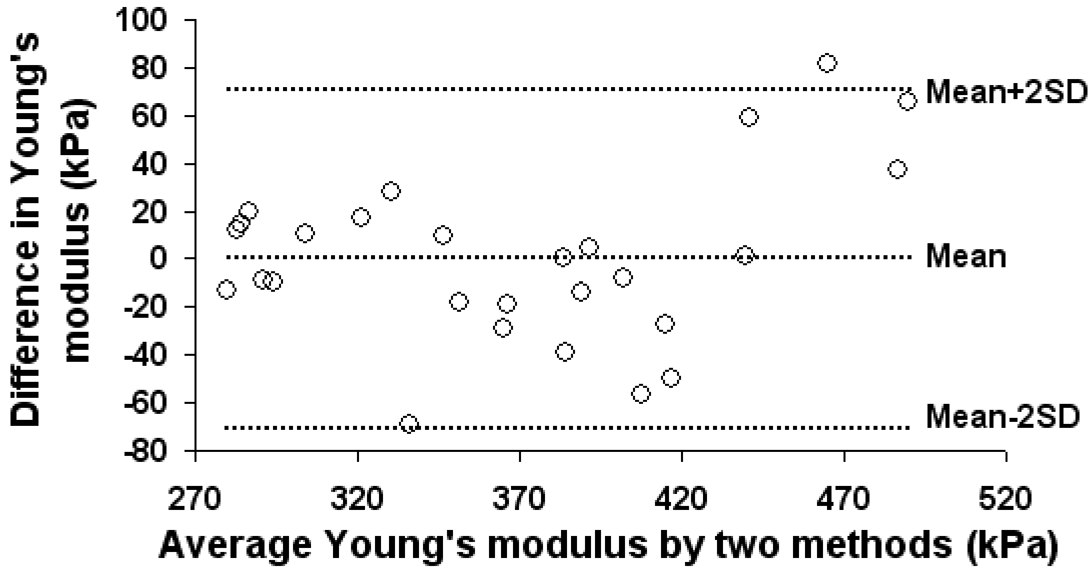
Difference in Young's modulus (kPa)
100
80
60
40
20
0
-20
-40
-60
-80
Mean+2SD
Mean
Mean-2SD
270
320
370
420
470
520
Average Young's modulus by two methods (kPa)

Figure 10.

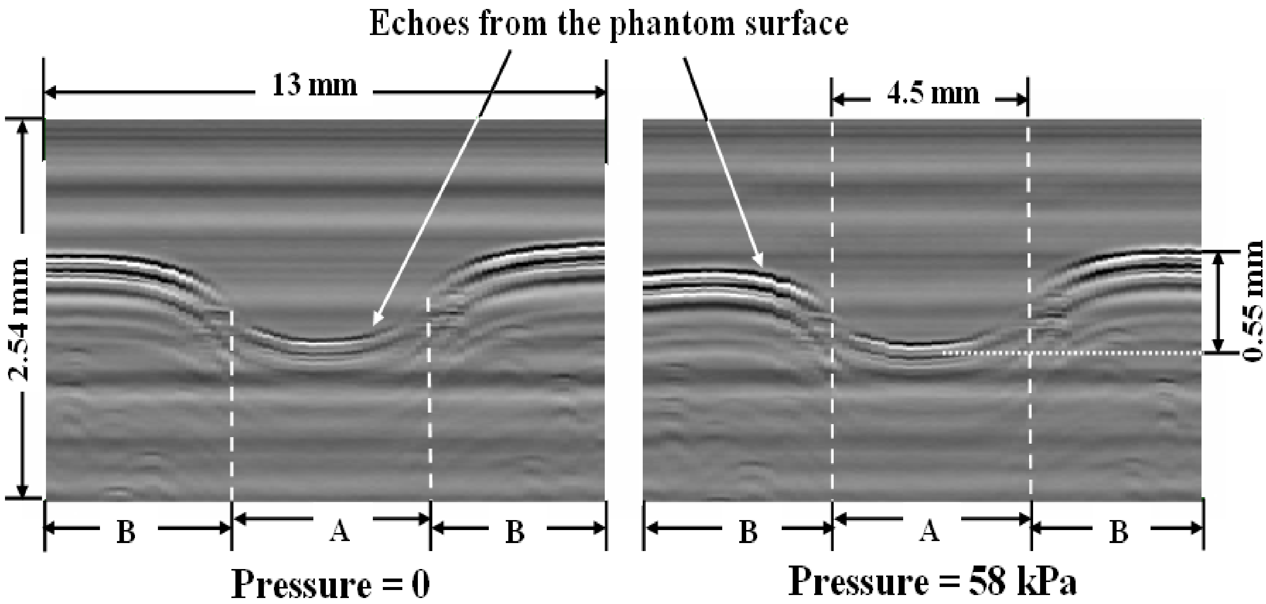

Figure 11 (a).

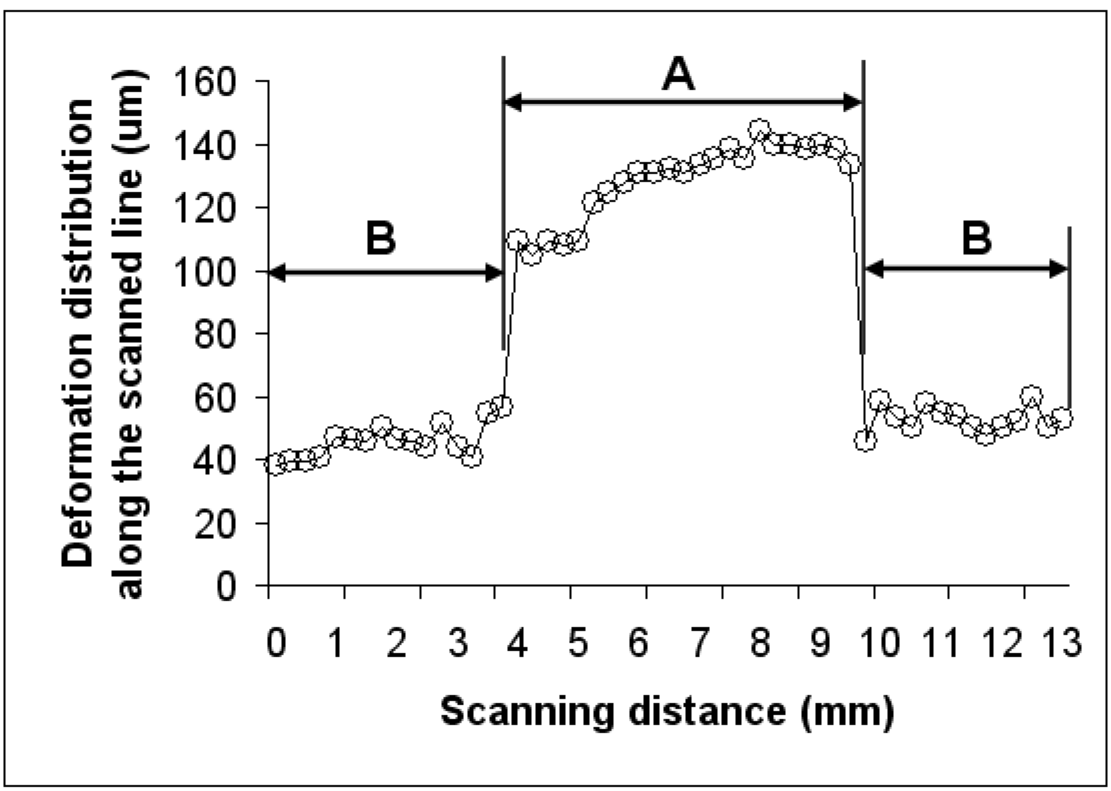

Figure 11 (b).